A Silicon Microring Optical 2x2 Switch Exploiting Orbital Angular Momentum for Interconnection Networks up to 20Gbaud

Mirco Scaffardi, Muhammad N. Malik, Emma Lazzeri, Gianluca Meloni, Francesco Fresi, Luca Potì, Nicola Andriolli, Isabella Cerutti, Charalambos Klitis, Laura Meriggi, Ning Zhang, Marc Sorel, Antonella Bogoni

***Abstract*—The orbital angular momentum (OAM) of light can be exploited as an additional switching domain together with more traditional switching domains as wavelength, space and time to implement multi-layer interconnection networks with high capacity, low power consumption and fast reconfiguration time. In this work we propose a two-layer optical interconnection network exploiting OAM and wavelength as switching domains. The key component of the interconnection network is the OAM-based switching element, here implemented on a silicon-on-insulator chip exploiting microrings. This implementation allows fast tuning (down to nanosecond range) and low power consumption (a few tens of mW per microring). We report the first implementation of an OAM-based 2x2 switch exploiting a dual-grating microring. The measurements are taken for OOK and 16QAM input signals modulated up to 35Gbaud. A bit error rate below the forward error correction threshold is demonstrated up to 20Gbaud for all the switching scenarios, with power penalty <1dB with respect to the back-to-back. A characterization of the integrated microring is carried out also in terms of beam divergence for different radii and emitted OAM orders. The characterization has brought to an empirical model which can aid the microring design in order to optimize the collimation of the OAM beams through the interconnection network.**

***Index Terms*—Microring, optical vortex, interconnection networks, orbital angular momentum.**

I. Introduction

The growth of the internet traffic is causing a corresponding growth of data centres, which employ a large number of servers connected by a complex network infrastructure. The scalability of current electrical interconnection networks will be soon limited by their power consumption and related power dissipation and footprint issues [1, 2]. Optical switching offers a very effective solution to overcome the aforementioned issues as it enables the realization of high capacity and reconfigurable interconnection networks with low power consumption [3-5]. The scalability of the optical interconnection networks can be enhanced by exploiting multiple switching domains. Multi-plane interconnection networks are composed of a number of cards, each of them supporting a number of ports, which are optically interconnected. The traditional switching domains envisioned for a flexible switching of data packets across all ports and cards are space, wavelength, and time [6-9]. The orbital angular momentum of light represents a novel domain that can be exploited alone or in combination with the other switching domains to improve the scalability and performance of the multilayer interconnection networks. An optical beam with OAM of order l, where l is an integer, has an azimuthal phase term $exp(i \cdot l \cdot \theta)$, where θ is the azimuthal angle. Beams with different OAM order are orthogonal, i.e. they can propagate together ideally without crosstalk [10]. These characteristics make OAM of light very attractive as a further multiplexing domain to improve the switching capacity. Moreover conversion between OAM modes is a linear and passive process [11] and therefore it does neither introduce noise, nor change the photon energy, nor require supply of energy. This makes the OAM switching energy-efficient and practical to implement. The OAM has been exploited as single layer switching domain in [12] where an access passive optical network architecture is proposed, where different optical network units are addressed with OAM beams of different order. OAM can be impressed to a Gaussian beam by means of bulky passive devices such as spiral phase plates [13] or active devices such as commercial spatial light modulators (SLMs) [10]. A reconfigurable 2x2 optical switch has been demonstrated in [14, 15] based on these devices. Integrated devices such as microrings with super-imposed grating [16, 17] circular grating couplers cascaded to star couplers [18] and hybrid 3D integrated circuits [19] have been recently demonstrated as a more compact alternative to the generation of light carrying OAM. Integrated devices are attractive for the small form factor (i.e. typical widths of tens of micrometers), fast tunability and low-power consumption (i.e. μs timescale and tens of mW with thermal tuning) [17]. Therefore, integrated photonics offers a very attractive solution for the development of effective and practical OAM-based optical switches. In this paper we demonstrate, for the first time, the use of a silicon-on-insulator dual-grating micro-ring as optical 2x2 switch based on orbital angular momentum

Manuscript received September 15, 2016. This work has been done within the Project ROAM-Revolutionizing optical fiber transmission and networking using the orbital angular momentum of light (Call ID: H2020-ICT-2014-1; topic: ICT-06-2014; funding scheme: RIA; contract number: 645361) and partially supported by the project MINOS (FIRB-RBFR12N2T9).

M. Scaffardi, M. N. Malik, G. Meloni, L. Potì are with are with CNIT, via G. Moruzzi 1, 56124, Pisa (corresponding author e-mail: mirco.scaffardi@cnit.it).

E. Lazzeri, F. Fresi, N. Andriolli, I. Cerutti, M. N. Malik and A. Bogoni are with Scuola Superiore Sant'Anna, Via Moruzzi 1, 56124 Pisa, Italy.

C. Klitis, L. Meriggi, Ning Zhang, M. Sorel are with University of Glasgow, Oakfield Avenue, Glasgow G12 8LT, UK .

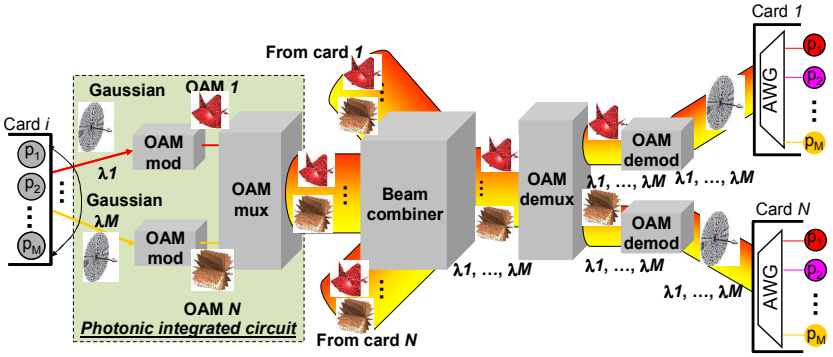

Fig. 1 Two-layer interconnection network based on the NxM switch exploiting M OAM modes and N wavelengths. AWG: arrayed waveguide grating.

and wavelength. The simultaneous exploitation of the OAM and wavelength domains allows to increase the network scalability and energy efficiency, while avoiding the complexity of the state-of-the-art optical space switching. We report results on BER measurements of the 2x2 switch for OOK and 16-QAM coherent traffic up to 20 Gbaud/s.

The two-layer interconnection network proposed in this work exploits several multiplexed OAM beams generated by independent microrings. In order to propagate the multiplexed OAM beams collimation is necessary, and the small form-factor allows to package the microrings together with micrometer-scale lenses. Therefore, the knowledge of OAM beams divergence is necessary for a proper design of the system of lenses for OAM beam collimation and transmission. So far the divergence of OAM beams has been investigated, focusing on the generation of OAM beams from a Gaussian beam, both theoretically [20] and experimentally [21, 22] with a set of four OAM modes. Nevertheless, the divergence of optical vortices emitted by integrated microrings have not been thoroughly investigated yet. A characterisation is made for two OAM modes and for a single microring [23].

This paper proposes a characterisation of the divergence of the OAM beams emitted by integrated microrings. With respect to previous works [23], the characterization is made for several OAM orders and different ring radii. We also develop an empirical model to predict the OAM beam divergence as a function of the OAM order and the ring radius. The model provides guidelines for the design of integrated microrings and the dimensioning of the lens system for the transmission of the emitted OAM beam.

The manuscript is organized as follows. Section II describes the two-layer interconnection network based on OAM and wavelength switching domains. Section III introduces the architecture of the 2x2 OAM switch. Section IV describes the experimental switch characterization and the measured performance. In Section V the divergence of the OAM beams emitted from the microrings is investigated. The conclusions are drawn in Section VI.

II. Interconnection Network

The proposed two-layer OAM-based interconnection network is shown in Fig. 1. The scheme origins from a previous architecture not exploiting the OAM as switching domain [24], where N independent line cards each one with M input/output ports (p_1,…,p_M) are interconnected. Here we propose to implement the switching among the ports in the wavelength domain, i.e. the destination port is determined by the wavelength of the transmitted signal, while the switching among the cards is implemented in the OAM domain. More specifically, while in [6-8, 24] the destination card is addressed through an optical space switch, in this work the destination card is selected by a different OAM mode for each signal coming from one of the card input ports. The selected OAM mode unambiguously determines the destination card, independently of the signal wavelength. The control of the interconnection network can be achieved with the scheduling framework described in [25], which determines the wavelength to be assigned to each card input, and the OAM mode to be assigned to each card. The part of the interconnection network highlighted in green can be realized through a photonic integrated circuit that includes N replicas of M concentric microrings with imposed grating, each acting as an independent OAM mode emitter [26]. Each concentric set of microrings serves a specific card, and each ring serves a specific port. Each ring generates the desired OAM mode which is co-axially emitted with the other generated OAM modes, providing the multiplexed beams. The small form-factor of the microrings allows them to be packaged together with micrometer-scale lenses and beam combiners for beam collimation and manipulation. Thermo-optical or current-injection effects can be exploited to independently tune the OAM mode emitted by each ring to ensure a complete switching flexibility. OAM demultiplexers can be implemented with a passive device based on a multiplane light converter [27] or with a couple of patterned polymethyl methacrylate-based lenses [28].

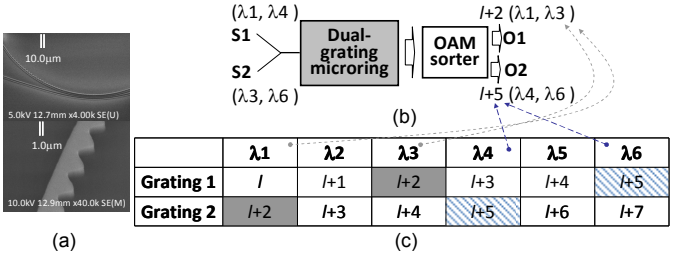

	λ1	λ2	λ3	λ4	λ5	λ6
Grating 1	*l*	*l*+1	*l*+2	*l*+3	*l*+4	*l*+5
Grating 2	*l*+2	*l*+3	*l*+4	*l*+5	*l*+6	*l*+7

Fig. 2 (a) Microscope image of the dual-grating SOI microring. (b) Scheme of a 2x2 OAM-based switch exploiting a dual-grating microring and an OAM mode sorter. (c) Mapping of the emitted OAM mode order *l* for the two gratings vs. wavelength λi of the resonance peaks.

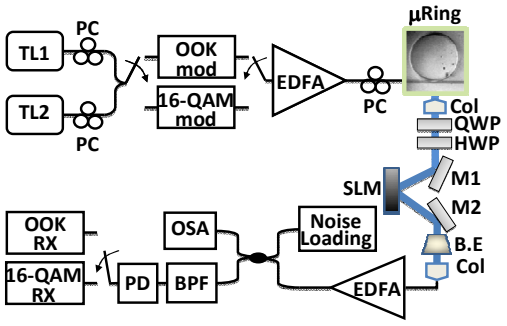

Fig. 3 Experimental setup. TL: tunable laser. mod: modulator. EDFA: erbium doped fibre amplifier. OSA: optical spectrum analyser. PC: polarisation controller. Col: collimator. QWP: quarter wave plate. HWP: half wave plate. M: mirror. B. E.: beam expander. BPF: band pass filter. RX: receiver.

The wavelength demux is realized through arrayed waveguide grating (AWG) filters.

III. OAM-BASED 2X2 OPTICAL SWITCH ARCHITECTURE

A simplified geometry for an OAM modulator/multiplexer consists of a single microring with superimposed multiple gratings, where each grating is designed to emit a pre-defined OAM mode at a given input wavelength set at one of the resonances of the microring [29]. The mechanism of OAM emission lies in the fact that the light is emitted at an angle with respect to the chip plain due the presence of gratings on the internal ring sidewall. Since the waveguide is curved, the wavefront of the radiated light skews in the azimuthal direction and transforms into a helix, thus generating an OAM beam. The order of the emitted OAM beam, is equal to the difference between the number of optical periods of the light circulating into the ring and the number of grating elements of the resonator [16]. Fig. 2 (a) shows the picture a dual-grating microring. The general scheme of the 2x2 OAM-based switch exploiting a dual-grating microring is shown in Fig. 2 (b). Two signals S1 and S2 are coupled and fed to a dual-grating ring where they are converted to an OAM beam with order l and $l+\Delta q$, where Δq is the difference between the number of grating elements of the two gratings [29]. The OAM beams, which co-propagate coaxially in the free-space, are then sent to an OAM mode sorter, which demultiplexes them depending on the order of the OAM beam. In our implementation the single Si-based microring has two overlapped gratings with Δq=2, radius of 29µm and a free spectral range of ~3nm. Fig. 2 (c) shows the mapping of the emitted OAM mode order l for the two gratings vs. the wavelength λi of the resonance peaks. A set of two wavelengths can be assigned to S1 and S2 in order to implement a non-blocking 2x2 switch. In fact each wavelength corresponds to a different OAM order l, which, in turn, is associated to one of the output ports. A possible couple of OAM modes have order l+2 and l+5. According to Fig. 2 (c) these modes can be selected by assigning wavelengths λ1 and λ4 to S1 and λ3 and λ6 to S2. Since the couple of wavelength associated to S1 is different from the couple of wavelength assigned to S2, both the input signals can be directed to the same output port, allowing for four switch configurations. More wavelength flexibility could be obtained with a higher number of gratings per ring. For example, with a four-gratings ring with Δq=1, two different sets, each with four different wavelengths, can be assigned to S1 and S2, i.e. two wavelengths can be associated to each destination port for each input port. Increasing the number of gratings on the ring does not influence the purity of the emitted OAM modes until the resolution limit of the grating writing process is reached [30]. Nevertheless, the power of each emitted mode is reduced since the total emitted power is split on a larger number of modes. The use of a single multi-grating microring instead of multiple concentric microrings does not allow for the independent tunability of the OAM modes emitted by each grating, preventing a complete switching reconfigurability and full wavelength flexibility. Nevertheless, the single multi-grating ring requires a single input optical coupling, thus reducing the complexity of a laboratory proof-of-concept demonstration without packaging. The similarity between the structures of a multi-ring OAM modulator/multiplexer and a multi-grating ring OAM modulator/multiplexer allows the demonstration of the operating principle of the proposed two-layer switching architecture, providing an initial performance assessment.

IV. IMPLEMENTATION

In this section the implementation and characterization of the 2x2 OAM-based switch is described.

TABLE I
CONFIGURATION STATES OF THE 2X2 OAM SWITCH

State	S1 [nm]	S2 [nm]	Switch	Output
1	1542	1557	S1→O1, S2→O2	l=10; l=13
2	1542	1547	S1→O1, S2→O2	l=10; l=10
3	1551	1547	S1→O1, S2→O2	l=13; l=10
4	1551	1557	S1→O1, S2→O2	l=13; l=13

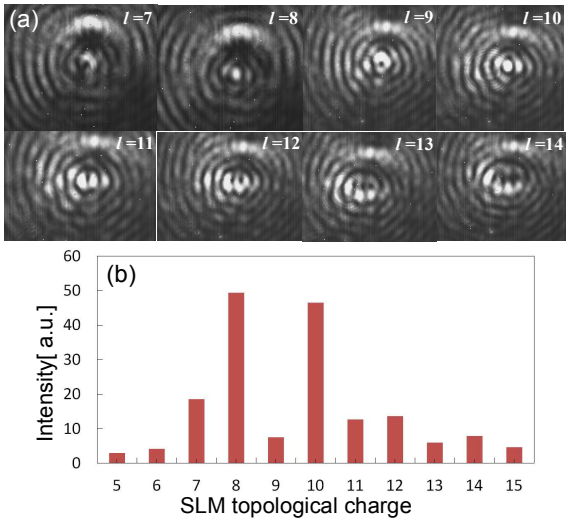

Fig. 4 Evaluation of the purity of the demodulated OAM modes after SLM diffraction. (a) Pictures at the infrared camera for different topological charges of the SLM phase mask. The topological charge of the loaded phase mask is indicated. (b) On axis intensity of the radiation registered by the infrared camera vs. the different topological charges of the demodulating phase masks loaded on the SLM. The input signal wavelength is fixed to 1542.2nm.

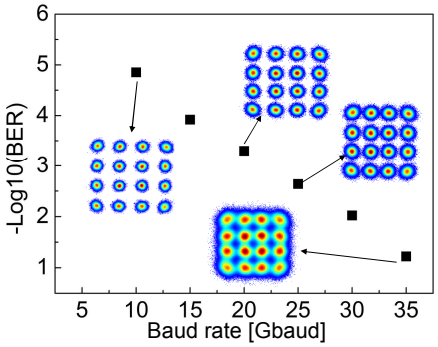

Fig. 5 BER vs. baud rate for a 16QAM signal at 1542.2nm (*l*=10).

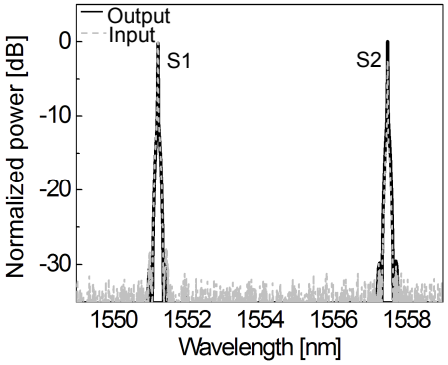

Fig. 6 Power spectrum at dual-grating microring input and output for S1 and S2 with OOK modualtion at 20Gbaud.

A. Experimental setup for switch characterization

The experimental setup is shown in Fig. 3. The input signals are generated from two tunable lasers. For OOK signal generation the tunable lasers are fed into a Mach-Zehnder amplitude modulator driven by an electrical PRBS 2^{31}-1. The 16QAM signal is generated with an IQ modulator driven by two decorrelated 2^{11}-1 PRBSs. Each transmitter emits two signals S1 and S2 at wavelength 1542.2 or 1551.2nm for S1 and 1547.9 or 1557.5nm for S2. An EDFA sets the power at the microring input at 25dBm in order to compensate for the coupling losses, the microring losses, and the losses of the passive free-space elements. The signal is fed into the microring with a tapered fiber with spot size 5µm. Each signal S1 and S2 is emitted from the microring with an OAM of order *l* and *l*+2 depending on the input wavelengths and propagates collimated in free space along a direction orthogonal to the chip plane. A spatial light modulator (SLM) (Holoeye Pluto Telco-013) converts a selected OAM mode back to a Gaussian beam. In order to optimize the conversion efficiency, a quarter wave plate (QWP) and an half wave plate (HWP) are employed. The OAM mode conversion operation is performed independently of the signal wavelength. The size of the Gaussian beam is then enlarged with a beam expander (BE) to couple it into a standard fibre with a focusing lens. The signal is then amplified, loaded with noise and filtered (BPF) before being received. The spectrum is monitored with an optical spectrum analyzer (OSA).

B. Performance

The configuration states of the OAM-based 2x2 switch based on a dual-grating ring are shown in Table 1.

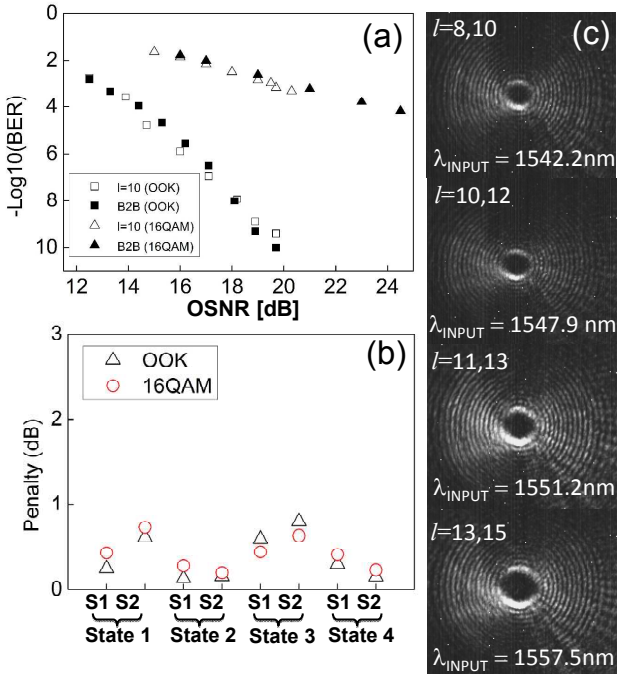

Fig. 7 (a) BER vs. OSNR at 20Gbaud (*l*=10, S1) for OOK and 16QAM modulation. Back-to-back and signal S1 at output for *l*=10 (1542.2nm). (b) BER penalty with respect to back-to-back for the 16QAM (at BER=10^{-3}) and OOK (at BER=10^{-9}) modulation format at 20Gbaud. All the switch configuration states are shown. (c) Far-field intensity of the emitted OAM modes for the 4 input wavelengths.

Output ports O1 and O2 are addressed with OAM of order 10 and 13 respectively. Mode 10 is generated at 1542.2nm (S1, grating2) and 1547.9nm (S2, grating1), while mode 13 is generated at 1551.2nm (S1, grating2) and 1557.5nm (S2, grating1). We first evaluated the purity of the OAM modes generated by the dual-grating microring. The wavelength is set to 1542.2nm, where the modes with *l*=8 and 10 are emitted. The SLM (see Fig. 3) is loaded with a phase mask of topological charge ranging from 5 to 15 and the on axis intensity registered by an infrared camera after a focusing lens. Fig. 4 (a) shows the intensity registered by an infrared camera for demodulated OAM modes of different order *l*. A central bright circle is clearly visible for the cases l=8 10, confirming that the corresponding OAM beams are converted to a gaussian beam. In Fig. 4 (b) the intensity for each value of loaded topological charge is registered. More than 60% of the total power is converted to OAM modes 8 and 10. Improvement of the converted power for modes 8 and 10 is expected with an optimized alignment of the free-space optical setup. The performance of the OAM-based 2x2 switch is investigated for both 16QAM and OOK modulation formats. First, the bandwidth of the microring has been characterized and the results are show in Fig. 5. The BER vs. the baud rate for the dual-grating ring is plot for a 16QAM input signal at 1542.2nm (OAM mode of order *l*=10 is observed) and constant OSNR of 20dB. The constellations are shown for few selected relevant cases including the lowest and highest baud rates. A baud rate of 20Gbaud is the limit for a BER=10^{-3} (forward error correction threshold) and clear constellation. The BER degradation for higher baud rates is due to the filtering operated by the microring, which cuts part of the input signal spectrum. The power spectra at the input and

output of the dual-grating microring are also measured when 20Gbaud OOK signals at 1551.2nm (S1) and 1557.9nm (S2) are at the input and shown in Fig. 6. The picture shows that the spectra are unaltered by the microring filtering function. Two complete BER curves are shown in Fig. 7 (a) for the back-to-back (filled symbols) and for S1 (empty symbols) modulated at 20Gbaud with OOK (squares) and 16QAM (triangles) modulation format. Performance is measured by demodulating OAM mode of order l=10. The back to back measurements are taken by replacing the microring and the free-space chain with a band pass filter of about 0.2nm bandwidth, i.e. equal to the one of the microring. The back to back performance is in few cases slightly worse than the switch output due to the not perfect matching of the filter shape with the shape of the microring filtering function. Fig. 7 (b) shows the power penalty with respect to the back-to-back at BER=10^{-9} and 10^{-3} for OOK (triangles) and 16QAM (circles) modulation format respectively, for all the switch configuration states and all the input signals S1 and S2. A maximum penalty of 1dB is measured, indicating similar performance for all the configuration states. The far field intensity of the OAM modes emitted by the dual-grating microring for the 4 input wavelengths is shown in Fig. 7 (c). In order to evaluate the performance for different emitted OAM modes, i.e. at different resonances, we evaluated the BER for a 10Gb/s OOK signal at different wavelengths, i.e. from mode 5 to 14, on a microring of radius 29μm, i.e. the same free spectral range, with a single grating. Fig. 8 shows that the maximum penalty at BER=10^{-9} is less than 2dB. This demonstrates that the two-layer switch based on integrated microrings for OAM modulation and multiplexing can work for a wide range of wavelengths, almost covering entirely the C-band.

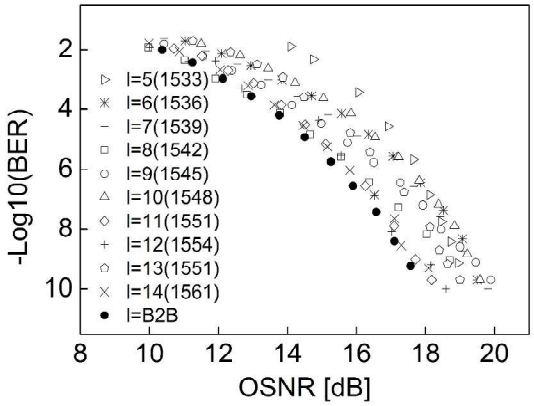

Fig. 8 BER vs. OSNR at different resonance wavelengths (OAM mode) for a 10Gb/s signal modulated with an OOK PRBS 2^{31}-1.

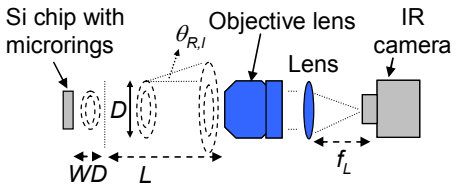

Fig. 9 Experimental setup for the beam divergence characterization. *WD*: working distance; *L*: displacement between objective and the working distance at which the chip is at focus. f_L: focal length of the lens. *D*: external diameter of OAM beam intensity distribution. $\theta_{R,l}$: divergence angle.

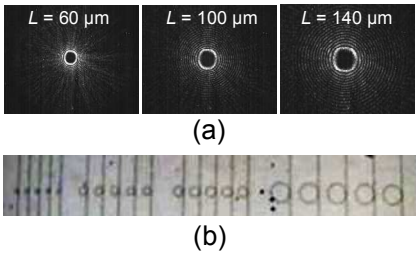

Fig. 10 (a) Intensity distribution at the IR camera of the OAM beam (l=15) emitted by the ring with R=37.9 μm for L=60, 100 and 140 μm. (b) Microscope image of the silicon chip with the integrated microrings [16].

V. OAM BEAM DIVERGENCE CHARACTERIZATION

For practical use of the OAM-based components, packaged solutions are required. One of the main critical aspects of the packaging of the OAM emitters, i.e. microrings, is the beam collimation through microlenses. For this reason a characterization of the integrated microring is carried out also in terms of beam divergence for different radii and emitted OAM orders and reported in this section. The characterization has brought to an empirical model to be employed in the microring design for optimizing the collimation of the OAM beams through the interconnection network.

A. Experimental setup for OAM beam divergence characterization

The experimental setup for the characterization of the OAM beam divergence is shown in Fig. 9. A silicon chip comprising multiple microrings with different radii is mounted on a precision stage with two translational axes and a rotational axis. Light generated by a tunable laser is injected into the microring input waveguide through butt coupling by means of a cleaved single-mode fibre pigtail. The waveguide has a tapering section for improved coupling efficiency. The light coupled into the ring is converted to an OAM beam thanks to an angular grating defined on the ring waveguide and emitted perpendicularly to the ring plane [16]. The OAM beam is collected with an objective lens with numerical aperture (NA) 0.65, effective focal length (EFL) 4.5 mm, working distance (WD) 0.6 mm placed at a distance WD+L from the ring. The objective collimates the beam to infinity. A lens (f_L: 200 mm) focuses the beam on the CCD of an InGaAs infrared camera (pixel pitch 30 μm). When the objective is at distance WD, the near field of the emitted light is imaged on the camera. The distance between the objective and the ring is increased until the far-field is imaged. As an example, Fig. 10 (a) shows the intensity distribution of OAM beam of order l=15 emitted by the ring with radius R=37.9 μm for L=60, 100 and 140 μm. The external diameter D of the annular intensity distribution of the OAM beam at distance L is reconstructed from the diameter D_{IR} (number of pixels) measured on the IR camera, considering the magnification given by the system formed by the objective and the lens. The order l of the OAM light emitted by the microring is set by changing the wavelength [17]. The diameter D of the intensity distribution of the OAM beams as a function of L is measured for ring sets of four different radii R =[7.4, 15.7, 20.2, 37.9] μm shown in Fig. 10 (b). The rings are fabricated on silicon-on-insulator (SOI) substrate. Access and ring waveguides are 500-nm wide and 220-nm thick.

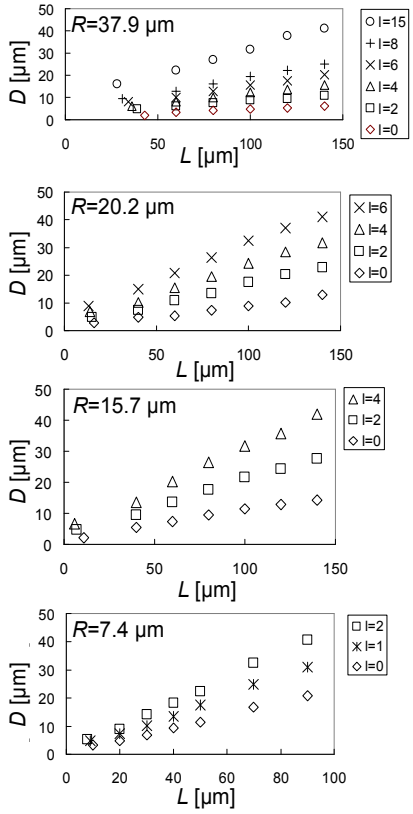

Fig. 11: Diameter D of the beam vs. distance L for different ring radii.

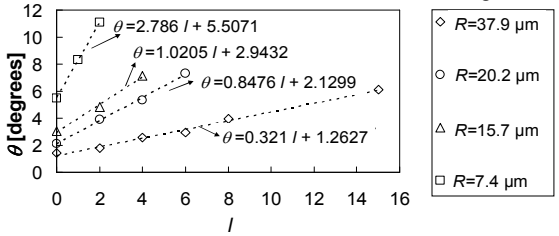

Fig. 12:. Calculated beam divergence $\theta_{R,l}$ for R = [7.4, 15.7, 20.2, 37.9] μm and l in the range [0-15]. The equation of the linear fitting function is reported.

The grating elements width is about 1/10 of the grating period. The structures are defined using electron-beam lithography followed by plasma etching. A 900-nm-thick SiO_2 layer is deposited onto the wafer [17].

B. Experimental results

Fig. 11 shows the beam diameter D as a function of the distance L for the different rings. The divergence $\theta_{R,l}$ is calculated for each ring of radius R and for a set of OAM orders l as an average as follows:

$$\theta_{R,l} = \frac{\sum_{i=1}^{N} \arctan\left(\frac{D_i - D_0}{2(L_i - L_0)}\right)}{N} \quad (1)$$

where N is the number of measurements, D_i and D_0 are the diameters of the annulus at distance L_i and L_0 (reference) respectively. Eq. (1) is derived from simple geometrical considerations. Fig. 12 shows the calculated beam divergence $\theta_{R,l}$ for R= [7.4, 15.7, 20.2, 37.9] μm and l in the range [0-15]. For rings with small radius, l is limited by the number of resonances of the transfer function within the C-band. As expected, the divergence increases with the OAM order l. Fixing l, the divergence increases when R decreases.

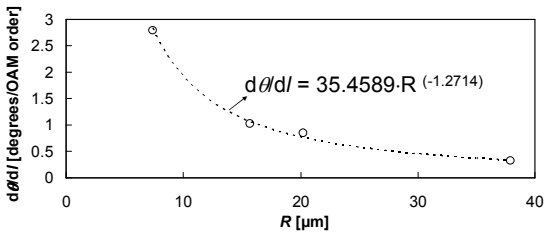

Fig. 13: Divergence slope (dθ/dl) vs. microring radius R.

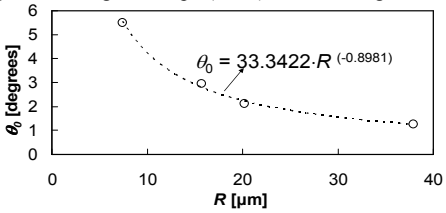

Fig. 14: Intercept θ_0 vs. microring radius R.

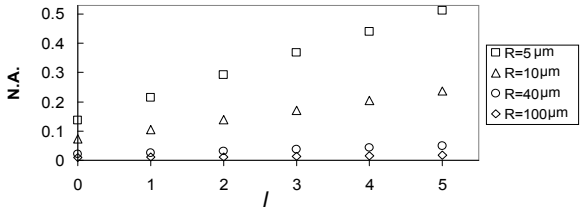

Fig. 15: Numerical aperture (NA) of the optical vortex vs l and R.

A linear fitting is performed for each set of divergence angles. The equations of the fitting functions are shown in Fig. 12 and have the general form of:

$$\theta_{R,l} = \frac{d\theta}{dl}(R)\cdot l + \theta_0(R) \quad (2)$$

A. Empirical equation for the divergence estimation of optical vortices

The dependence of the slopes and intercepts of the linear equations shown in Fig. 12 on the microring radius R is investigated in the following. Fig. 13 shows the slopes dθ/dl vs. R. The points are fitted with the exponential function reported in the figure. Fig. 14 shows the intercepts θ_0 of the fitting functions of Fig. 12. The intercept decreases with an exponential behaviour as a function of the microring radius.

Taking into account the dependence of dθ/dl and θ_0 on R according to Fig. 13, Fig. 14 and Eq. (2), the empirical equation for the estimation of the divergence of a vortex beam generated by the integrated microring can be written as:

$$\theta_{R,l} = \frac{35.4589}{R^{(1.2714)}}\cdot l + \frac{33.3422}{R^{(0.8981)}} \quad (3)$$

Eq. (3) can be used e.g. to estimate the minimum NA of a lens to collimate a vortex beam emitted by a microring. In Fig. 15 the NA of a microring emitting OAM beams with l = [0-5] is plotted for R = 5, 10, 40 and 100 μm. For R= 5 μm, a lens with NA>0.5 is necessary to collimate all the OAM beams. If R >40 μm, a lens with NA=0.05 allows the collimation of all the OAM beams. From this characterisation it results that for collimating in an effective way all the OAM beams emitted by a multiring-based OAM modulator/multiplexer with a single simple lens, it is more practical to design the rings with diameters very close and not too small and with low-order emitted OAM modes. This allows a single lens with small NA to collect all the light coming from each ring.

VI. CONCLUSIONS

We presented the architecture of an innovative optical two-layer interconnection network exploiting OAM and wavelength as switching domains. The network can be implemented with innovative SOI-based photonic integrated circuits based on microrings working as tunable OAM modulators and multiplexers. To demonstrate the feasibility of the presented interconnection network, we reported the first implementation and characterization of a 2x2 switch exploiting OAM and wavelength based on a dual-grating microring. The switch output ports are addressed with two OAM modes of different order. Performance is evaluated for 20Gbaud OOK and 16QAM signals for all the switch configuration states. A maximum penalty of 1dB is measured. The divergence of vortex beams generated with integrated silicon microrings is also extensively characterised in the C-band for different OAM orders and different microring radii in order to optimize the ring packaging for practical use. From the experimental results, a simple empirical model for the estimation of the divergence of a vortex beam is derived, which quantitatively determines the dependence of the divergence on the microring radius and the OAM order. This model can aid in the design of the microring-based OAM modulators and multiplexers optimizing the use of microlenses to be included in the device packaging. This work demonstrates the first implementation of an OAM-based switch exploiting integrated microrings for interconnection networks and shows that the OAM-based interconnection networks can be feasible with integrated packaged devices with low power consumption and fast reconfiguration speed.

REFERENCES

[1] K. G. Brill, "The invisible crisis in the data center: the economic meltdown of Moore's law," White Paper, *Uptime Institute*, 2007.

[2] J. Humphreys and J. Scaramella, "The impact of power and cooling on data center infrastructure," *Market Research Report*, IDC, 2006.

[3] D. A. B. Miller, "Device requirements for optical interconnects to silicon chips," *Proc. IEEE*, vol. 97, no. 7, pp. 1166–1185, July 2009.

[4] H. Cho, P. Kapur, K. Saraswat, "Power comparison between high-speed electrical and optical interconnects for interchip communication," *J. Lightwave Technol.*, vol. 22, no. 9, pp. 2021–2033, Sept. 2004.

[5] A. Benner, "Cost-effective optics: enabling the exascale roadmap," in *17th IEEE Symp. on High Performance Interconnects (HOTI)*, pp. 133–137, August 2009.

[6] N. Andriolli, P. G. Raponi, P. Castoldi, A. Bogoni, L. Potì, A. Bianchi; "Synchronous packet switches," PCT/EP2009/059412, WO/2010/127716, filed on Jul. 22, 2009, published on Nov. 11, 2010.

[7] R. Gaudino, G. Castillo, F. Neri, and J. Finochietto, "Can simple optical switching fabrics scale to terabit per second switch capacities?" *J. Opt. Commun. Netw.*, vol. 1, no. 3, pp. B56–B69, Aug. 2009.

[8] O. Liboiron-Ladouceur, I. Cerutti, P. G. Raponi, N. Andriolli, and P. Castoldi, "Energy-efficient design of a scalable optical multiplane interconnection architecture," *IEEE J. Sel. Top. Quantum Electron*., vol. 17, no. 2, pp. 377–383, Mar./Apr. 2011.

[9] O. Liboiron-Ladouceur, P. G. Raponi, N. Andriolli, I. Cerutti, M. Shafiqul Hai, and P. Castoldi, "Scalable Space–Time Multi-plane Optical Interconnection Network Using Energy-Efficient Enabling Technologies [Invited]", *J. Opt. Comm. Netw.*, vol. 3, no. 8, pp. A1-A11, August 2011.

[10] J. Wang, J.-Y. Yang, I. M. Fazal, N. Ahmed, Y. Yan, H. Huang, Y. Ren, Y. Yue, S. Dolinar, M. Tur and A. E. Willner, "Terabit free-space data transmission employing orbital angular momentum multiplexing", *Nature Photonics*, vol. 6, pp. 488-496, 2012.

[11] L. Allen, M. W. Beijersbergen, R. J. C. Spreeuw, J. P. Woerdma, "Orbital angular momentum of light and the transformation of Laguerre-Gaussian laser modes", *Physical Review A*, vol. 45, no. 11, pp. 8185-8189, 1992.

[12] Y. Fang, J. Yu, N. Chi, J. Zhang, J. Xiao, "A novel PON architecture based on OAM multiplexing for efficient bandwidth utilization", *IEEE Photonics Journal*, vol. 7, no. 1, 7900506, 2015.

[13] W. Xuli et al., "Orbital Angular Momentum Multiplexing in 0.1-THz Free-Space Communication via 3D Printed Spiral Phase Plates", Proc. *CLEO*, STu2F.2, San Jose, 2014.

[14] N. Ahmed, H. Huang, Y. Ren, Y. Yan, G. Xie, M. Tur, A. E. Willner, "Reconfigurable 2 × 2 orbital angular momentum based optical switching of 50-Gbaud QPSK channels", *Optics Express*, vol. 22, no. 1, pp. 756-761, 2014.

[15] A. E. Willner, L. Li, Guodong X., Yongxiong R., H. Huang, Y. Yue, N. Ahmed, M. J. Willner, A. J. Willner, Y. Yan, Z. Zhao, Z. Wang, C. Liu, M. Tur, S. Ashrafi, "Orbital-angular-momentum-based reconfigurable optical switching and routing", *Photonic Research*, vol. 4, no. 5, pp. B5-B8, 2016.

[16] X. Cai, J. Wang, M. J. Strain, B. Johnson-Morris, J. Zhu, M. Sorel, J. L. O'Brien, M. G. Thompson, S. Yu, "Integrated Compact Optical Vortex Beam Emitters", *Science*, vol. 338, 2012.

[17] M. J. Strain, X. Cai, J. Wang, J. Zhu, D. B. Phillips, L. Chen, M. Lopez-Garcia, J. L. O'Brien, M. G. Thompson, M. Sorel, S. Yu, "Fast electrical switching of orbital angular momentum modes using ultra-compact integrated vortex emitters", *Nature Comm*., vol. 5, no. 4856, 2014.

[18] N. K. Fontaine, C. R. Doerr, L. L. Buhl, "Efficient multiplexing and demultiplexing of free-space orbital angular momentum using photonic integrated circuits", in *OFC*, OTu1I.2, Los Angeles, 2012.

[19] C. Quin, B. Guan, R. P. Scott, R. Proietti, N. K. Fontaine, T. Su, C. Ferarri, M. Capuzzo, F. Clemens, B. Keller, M. Earnshaw, S.J.B. Yoo "Demonstration of Orbital Angular Momentum State Conversion using Two Hybrid 3D Photonic Integrated Circuits", in *OFC*, Th4A.1 San Francisco, 2014.

[20] M. J. Padgett, F. M Miatto, M. P J Lavery, A. Zeilinger, R. W Boyd, "Divergence of an orbital-angular-momentum-carrying beam upon propagation", *New Journal of Physics*, vol. 17, no. 023011, pp.1-4, 2015.

[21] S. G. Reddy, "Divergence of optical vortex beams", *Applied Optics*, vol. 54, no. 22, pp. 6690-6693, 2015.

[22] G. Xie, L. Li, Y. Yan, Y. Ren, Z. Zhao, P. Liao, N. Ahmed, Z. Wang, N. Ashrafi, S. Ashrafi, R. Linquist, M. Tur, A. Willner., "Performance Metrics for a Free-space Communication Link Based on Multiplexing of Multiple Orbital Angular Momentum Beams with Higher Order Radial Indices", in. *CLEO*, JTh2A.62, San Jose, 2015.

[23] L. Chen, J. Zhu, M. J. Strain, L. Meriggi, M. L. Garcia, K. Cicek, H. Li, X. Cai, M. Sorel, S. Yu "Measuring the angular emission of optical vortex beams from integrated devices", in *Group IV Photonics International Conference*, ThP24, Shanghai, 2014.

[24] I. Cerutti, N. Andriolli, P.G. Raponi, M. Scaffardi, O. Liboiron-Ladouceur, A. Bogoni, P. Castoldi, "Power and scalability analysis of multi-plane optical interconnection networks", *IET Optoelectron*, vol. 6, no. 4, pp. 192-200, 2012.

[25] P. G. Raponi, N. Andriolli, I. Cerutti, and P. Castoldi, "Two-step scheduling framework for space–wavelength modular optical interconnection networks," *IET Commun.*, vol. 4, no. 18, pp. 2155–2165, Dec. 2010.

[26] M. Sorel, M. J. Strain, S. Yu, X. Cai, "Photonic integrated devices for exploiting the orbital angular momentum (OAM) of light in optical communications", in *ECOC*, We.1.6.1, Valencia, 2015.

[27] J.-F. Morizur, L. Nicholls, P. Jian, S. Armstrong, N. Treps, B. Hage, M. Hsu, W. Bowen, J. Janousek, H.-A. Bachor. "Programmable unitary spatial mode manipulation". *Journal of the Optical Society of America A*, vol. 27, no. 11, pp. 2524-2531, 2010.

[28] H. Huang, G. Milione, M. P. J. Lavery, G. Xie, Y. Ren, Y. Cao, N. Ahmed, T. An Nguyen, D. A. Nolan, M.-J. Li7, M. Tur, R. R. Alfano, A. E. Willner, "Mode division multiplexing using an orbital angular momentum mode sorter and MIMO-DSP over a graded-index few-mode optical fibre", *Scientific Reports*, vol. 5, 14931, 2015.

[29] Q. Xiao, C. Klitis, S. Li, Y. Chen, X. Cai, M. Sorel, S. Yu, "Generation of photonic orbital angular momentum superposition states using vortex beam emitters with superimposed gratings", *Optics Express*, vol. 24, no. 4, pp. 3168-3176, 2016.

[30] M. J. Strain, S. Thoms, D. S. MacIntyre, M. Sorel, "Multi-wavelength filters in silicon using superposition sidewall Bragg grating devices", *Optics Letters*, vol. 39, no. 2, pp. 413-416, 2014.